X-641-71-421

PREPRINT

NASA TM X- 65726

APOLLO 15
X-RAY FLUORESCENCE EXPERIMENT

PRELIMINARY REPORT

OCTOBER 1971

GSFC — GODDARD SPACE FLIGHT CENTER —
GREENBELT, MARYLAND

X-641-71-421

X-RAY FLUORESCENCE EXPERIMENT

by

I. Adler,* J. Trombka, J. Gerard,**
R. Schmadebeck, P. Lowman, H. Blodgett,
L. Yin, E. Eller, and R. Lamothe

Goddard Space Flight Center

and

P. Gorenstein and P. Bjorkholm

American Science and Engineering

October 1971

GODDARD SPACE FLIGHT CENTER
Greenbelt, Maryland

*Principal investigator
**National Academy of Science (NRC)

CONTENTS

ILLUSTRATIONS

ILLUSTRATIONS (continued)

TABLES

X-RAY FLUORESCENCE EXPERIMENT

The X-Ray Fluorescence Spectrometer, carried in the SIM bay of the Command Service Module was employed principally for compositional mapping of the lunar surface while in lunar orbit, and secondarily, for x-ray astronomical observations during the trans earth coast. The lunar surface measurements involved observations of the intensity and characteristic energy distribution of the secondary or fluorescent x-rays produced by the interaction of solar x-rays with the lunar surface. The astronomical observations consisted of relatively long periods of measurements of x-rays from pre-selected galactic sources such as Cyg X-1 and Sco X-1 as well as from the galactic poles.

Principles and Theory

The production of x-rays characteristic of an element can be understood in terms of the simple Bohr picture of the atom. The electrons surround the nucleus in an orderly fashion in a series of shells K, L, M etc., as we move from the nucleus out towards the valence shell. For any given atom the binding energy of the inner electrons is greatest, decreasing as we move to the outer shells.

Because characteristic x-ray spectra result from the filling of the vacancies produced by the ejection of these inner shell electrons, greater input energy is required to excite the K spectrum than the L spectrum and still less energy is required for the M spectrum. The situation is summarized in Figure 1. In the table the absorption edge energies (E_k) are the energies required to ionize the atoms in the K shell and E ($K\alpha$) is the energy of the resulting x-ray line.

Thus, what is necessary is an incident energy in excess of the electron's binding energy in order to produce the characteristic x-rays.

In the Apollo experiment, described below, the production of the characteristic x-rays follows the interaction of solar x-rays with the lunar surface. It had appeared from a number of claculations that the typical solar x-ray spectrum is energetically capable of producing measurable amounts of characteristic x-rays from all the abundant elements up to about Z = 14(Si). During brief periods of more intense solar activity it should even be possible to observe radiation from elements of higher atomic number.

There are however some features of the sun's x-ray production which must be considered in some detail in the ultimate interpretation of the data. The solar x-ray flux exhibits a great deal of variability on time scales of minutes to hours. In addition there are systematic changes which are associated with the 11 year solar cycle.

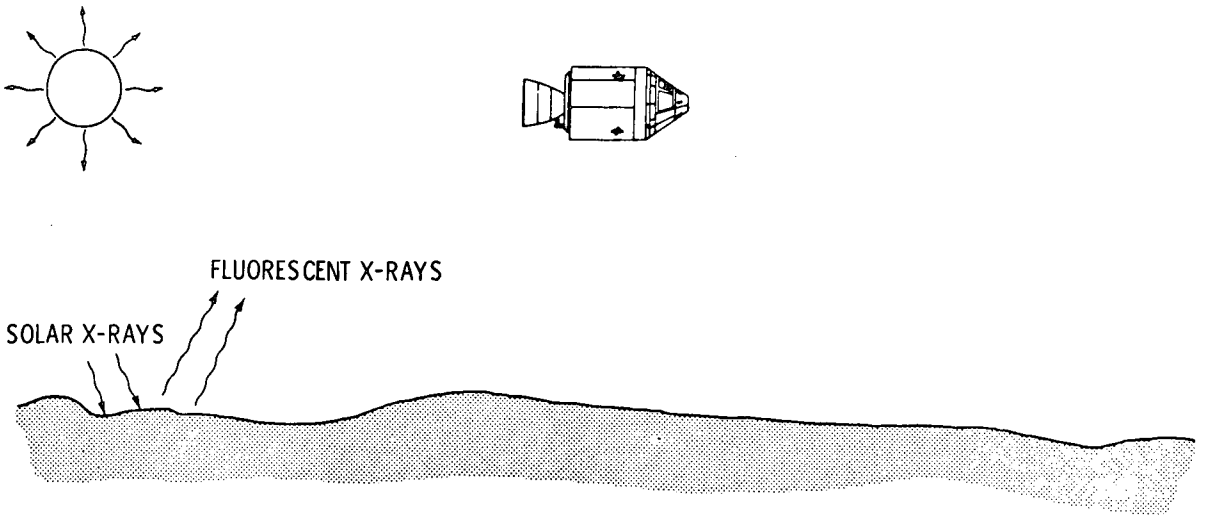

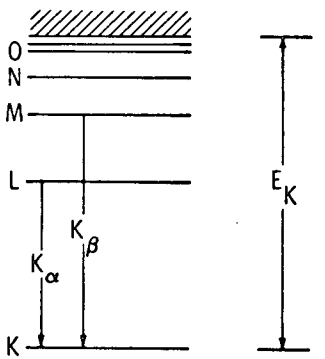

	$E(K_\alpha)$	ABSORPTION EDGES (E_K)
O	.54 KEV	
Fe	.73 KEV	
Na	1.04 KEV	
Mg	1.25 KEV	1.37 KEV
Al	1.49 KEV	1.57 KEV
Si	1.74 KEV	1.85 KEV
K	3.35 KEV	
Ca	3.70 KEV	

INNER ELECTRON TRANSITIONS GIVING
RISE TO CHARACTERISTIC K
X-RAY SPECTRA

Figure 1. X-ray fluorescence at the lunar surface.

Figure 2 shows this long term trend. A curve of the smoothed sun spot number is shown on the same axis. A definite correlation exists between the sun spot numbers and the x-ray intensity so that the extrapolated smoothed sun spot number can be taken as an indication of the expected solar intensity for the next few years.

It has been established that the solar x-ray flux, as one observes it with low resolution instruments such as proportional counters, decreases with increasing energy. If a strictly thermal mechanism of production is assumed, one finds variable coronal temperatures somewhere between 10^6 to 10^7 deg. K. Such variations in temperature produce both changes in flux and spectral composition. Thus one must expect changes not only in fluorescent intensities but in the relative intensities from the various elements being observed. For example should the solar spectrum harden (larger fluxes of higher energies) or should there be an increase in characteristic line intensities on the high energy side of the absorption edge of the heavier element, then we would observe an enhancement of the intensities from the heavier elements relative to the lighter ones.

In order to keep track of the possibly variable solar x-ray intensity and spectral shape an x-ray monitor was employed. In addition it was possible to obtain detailed simultaneous measurements of the solar x-ray spectrum from the various solrad satellites in flight during the mission.

Figure 3 shows an estimate of the emitted solar x-ray flux for an assumed temperature of 4×10^6 deg. K and a grey body emitter. Superimposed on this curve along the energy axis are the K shell absorption edges for Mg, Al, Si and K. Only the solar x-rays with energies on the high side of the absorption edges are capable of exciting those elements, and to a degree depending on the incident flux and the ionization cross section. Thus under quiet sun conditions the solar flux is most suitable for exciting the light elements. These include the major rock-forming elements Si, Al, and Mg.

Recognizing that the sun will produce secondary x-rays characteristic of such rock forming elements as Mg, Al and Si we then need to use equipment which measures both x-ray intensities and energies. Because the amounts of secondary x-rays produced are relatively small one cannot use a Bragg spectrometer for precise wavelength selection. Rather one is required to use low resolution but high sensitivity techniques such as proportional counters and pulse height analysis (1). To provide additonal energy discrimination selected x-ray filters are also employed (see below under instrument description).

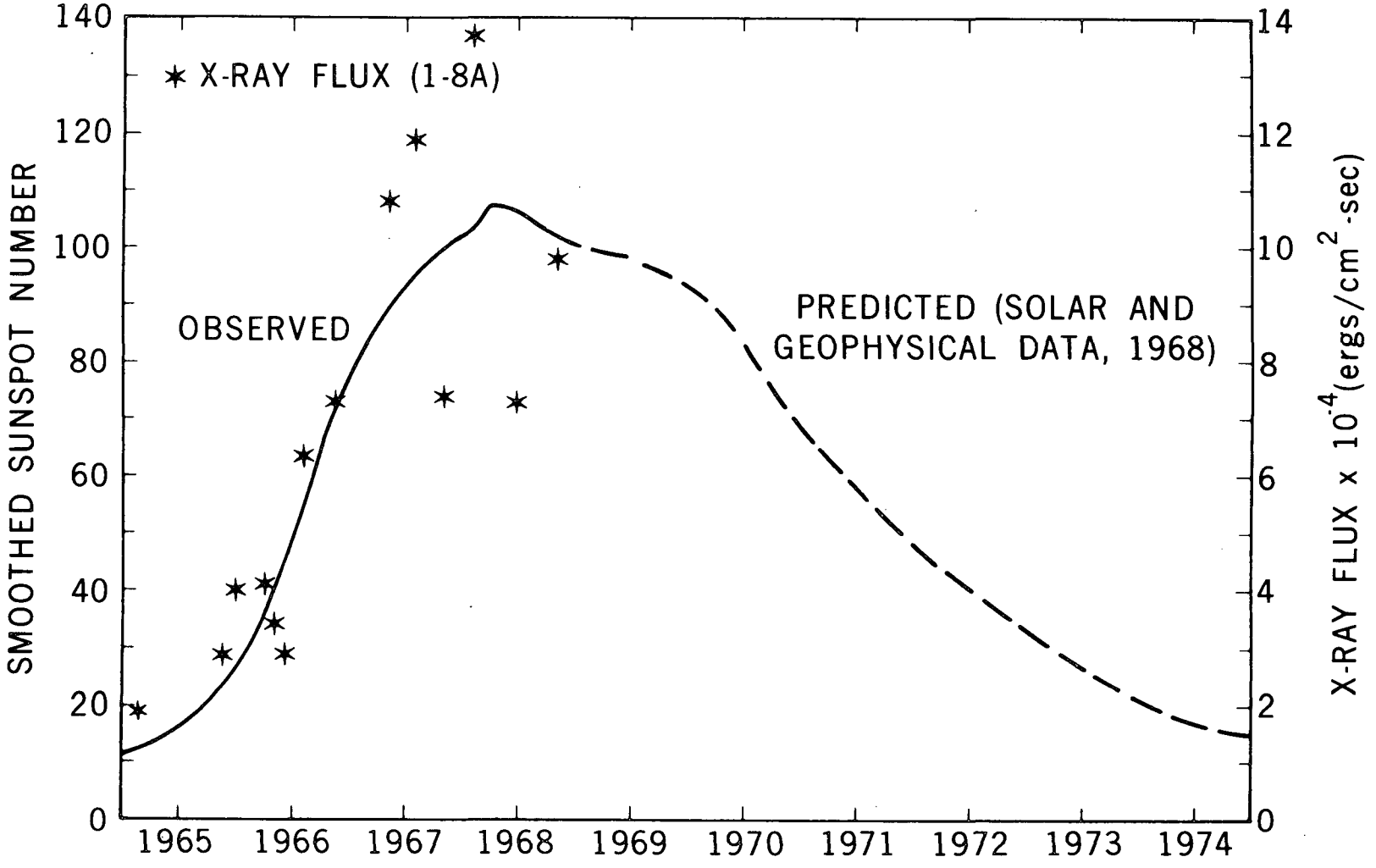

Figure 2. Smoothed sunspot number and observed X-ray intensity as a function of time during the solar cycle. These data and the extrapolated portion of the smoothed sunspot number curve have been obtained from various issues of Solar and Geophysical Data.

SOLAR SPECTRUM

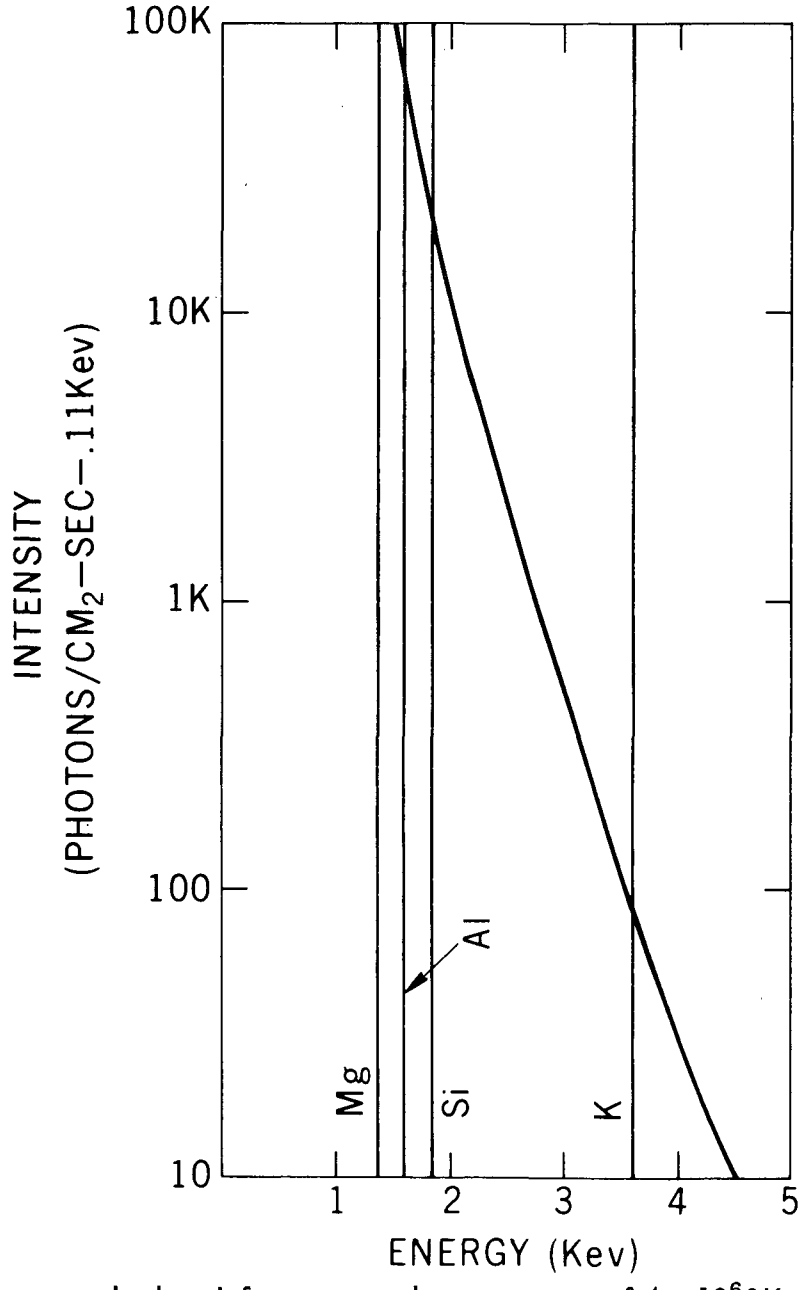

Figure 3. The solar spectrum calculated for a coronal temperature of 4×10^{6}°K. Superimposed are lines showing the positions of the absorption edges for Mg, Al and Si.

Description of the Instrument

A photograph of the instrument is shown in Figure 4 and in exploded view in Figure 5. It consists of three main subsystems:

(a) Three-large area proportional counters having "state of the art" energy resolution and 0.001-in. thick beryllium windows;

(b) A set of large area filters for energy discrimination among the characteristic x-rays of Al, Si and Mg;

(c) A data handling system for count accumulation, sorting into 8 pulse height channels and finally for relaying the data to the spacecraft telemetry.

Equipment Description

1. X-ray Detector Assembly: The x-ray detector assembly consists of three proportional counter detectors, two x-ray filters, mechanical collimators, an in-flight calibration device, temperature monitors and associated electronics. The detector assembly senses x-rays emitted from the moon's surface and converts them to voltage pulses which are processed in the x-ray processor assembly. Provisions for in-flight calibration are made through programmed calibration sources, which upon command, assume a position in front of the three detectors for calibration of gain, resolution and efficiency. Thermistors located at strategic points sense the temperature of the detector assembly for telemetry monitoring and temperature control of the detectors through heaters located near the proportional counter windows.

2. Proportional Counters: The three proportional counters are identical, each having an effective window area of approximately 25 cm^2 which consists of 0.001-in. thick beryllium. The proportional counters are filled to a pressure of one atmosphere with the standard P-10 mixture of 90 percent argon, 9.5 percent carbon dioxide, and 0.5 percent helium. Filters are mounted across the beryllium window aperature of two of the proportional counters to change the wavelength response. The filters consist of foils in the range of 0.2 to 0.5 mils thick; one being magnesium and the other aluminum. The third counter does not contain a filter. A single collimator assembly is used to define the field of view (FOV) of the three proportional counters as a single unit. The collimator consists of multi-cellular baffles, which combine a large sensitive area and high resolution but are restricted in the FOV. The

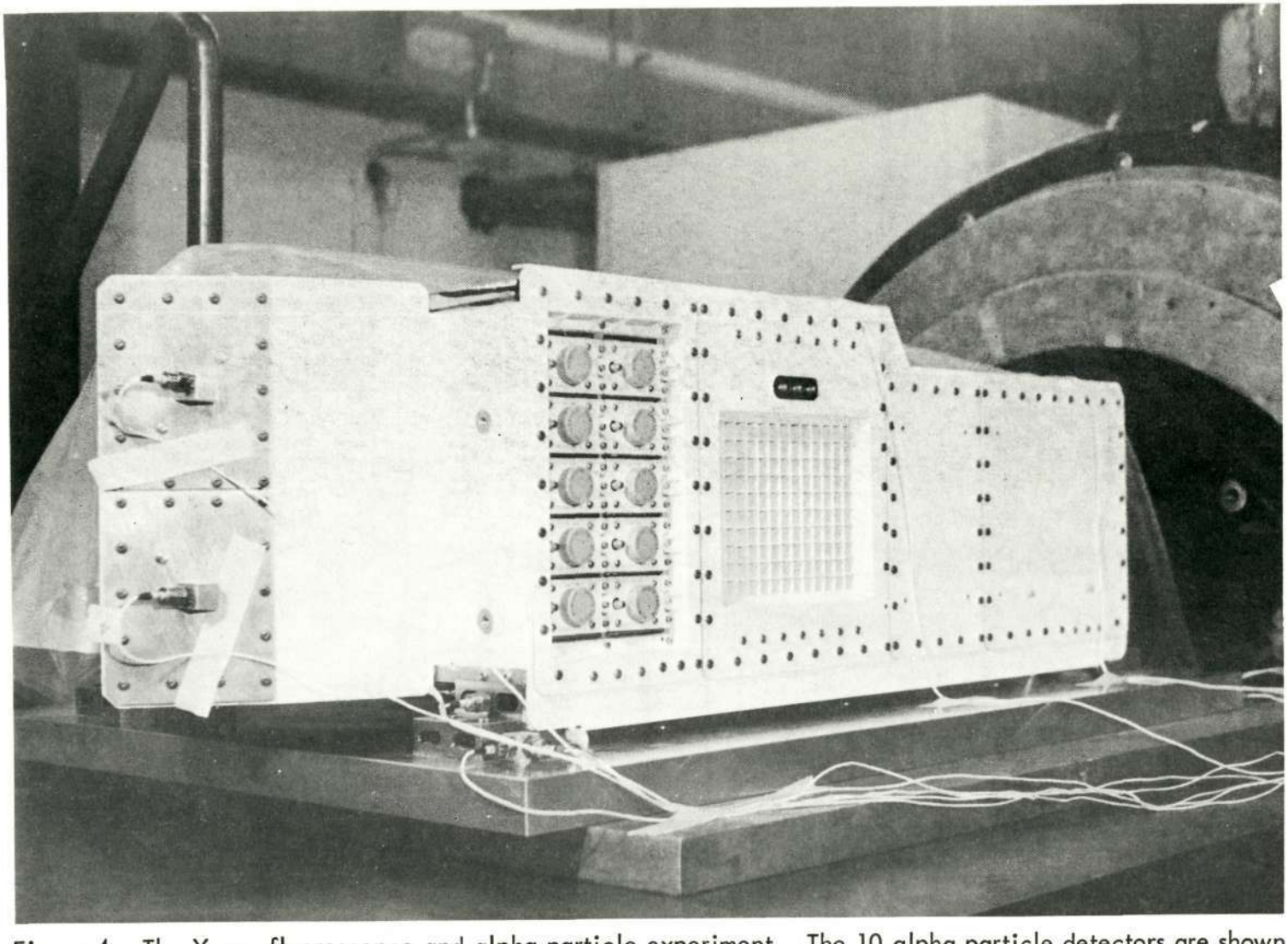

Figure 4. The X-ray fluorescence and alpha particle experiment. The 10 alpha particle detectors are shown to the left of the proportional counter collimator.

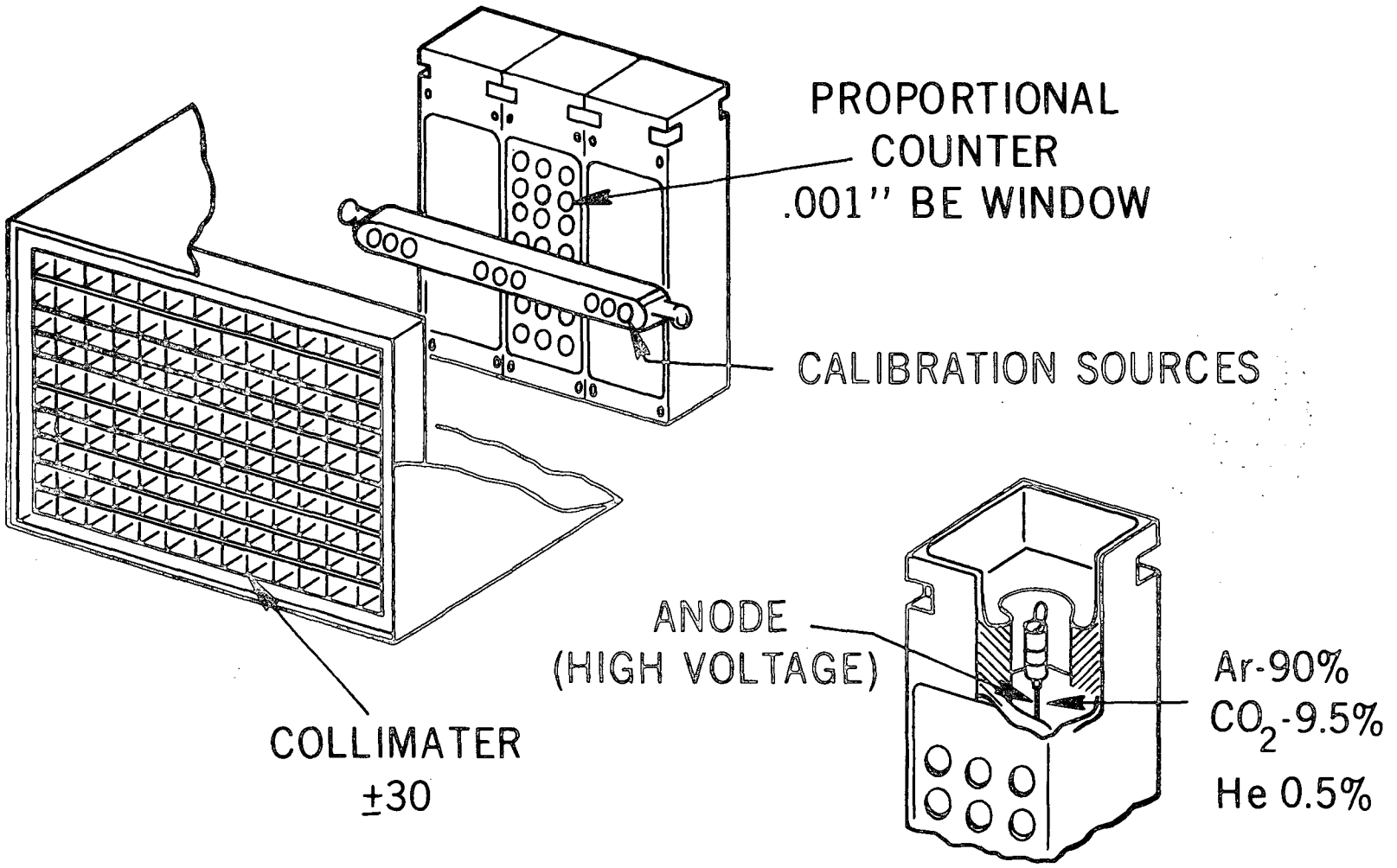

Figure 5. X-ray Spectrometer Functional Configuration

FOV determines the total flux recorded from the lunar surface and the spatial resolution. The FOV is specified as ±30 deg. full width half maximum (FWHM) in two perpendicular directions. The FWHM is the total angular width at which the collimator drops to one half of its peak response.

X-ray photons passing through a proportional counter beryllium window ionize the gas inside by an amount proportional to their energy. A very stable high voltage power supply provides a bias voltage for the operation of the proportional counters. This high voltage across the counter produces an electrical field gradient and hence a multiplication effect which results in a charge output that is proportional to the incident x-ray energy. Mounted on each proportional counter is a charge sensitive preamplifier which converts the imput charge to an output pulse by storing it on an integrating capacitor. This pulse has a fast rise time, determined primarily by the response of the preamplifier, a slow decay, determined by the integrator decay time, and an amplitude proportional to the x-ray energy. The preamplifier gain is set for an output scale factor of about 0.2 v/Kev. Each of the three preamplifier outputs are applied to the x-ray processor assembly which sorts the outputs according to the peak amplitude level.

3. In-Flight Calibration: The in-flight calibration device consists of a calibration rod with radioactive sources that normally face away from the proportional counters. Upon command from the x-ray processor assembly, the rod is rotated 180 deg. by a solenoid driver, thereby positioning the sources to face the proportional counters. Magnetically sensitive reed relays provide feedback signals indicating when the rod is fully in a calibrate mode or fully in the non-calibrate mode. These feedback signals are flag bits in the data telemetry output. The calibrate command signal is generated in the x-ray processor assembly. The calibration cycle repeats every 16 minutes and lasts for 64 seconds.

4. X-Ray Processor Assembly: The x-ray processor assembly processes x-ray data received from the detector assembly and the solar monitor. The lunar x-ray data is sorted, counted, stored and sent to telemetry. The solar x-ray data from the solar monitor is counted, stored and sent to telemetry. Processing of the data from one detector is shown in a functional block diagram in Figure 6. The pulse received from the charge sensitive preamplifier is amplified and operates up to eight voltage discriminators, depending on its voltage level. The discriminator outputs are processed logically in the pulse routing logic to obtain an output pulse in one of eight data channels, depending on the highest level discriminator operated. We thus obtain eight channels of differential pulse height spectra.

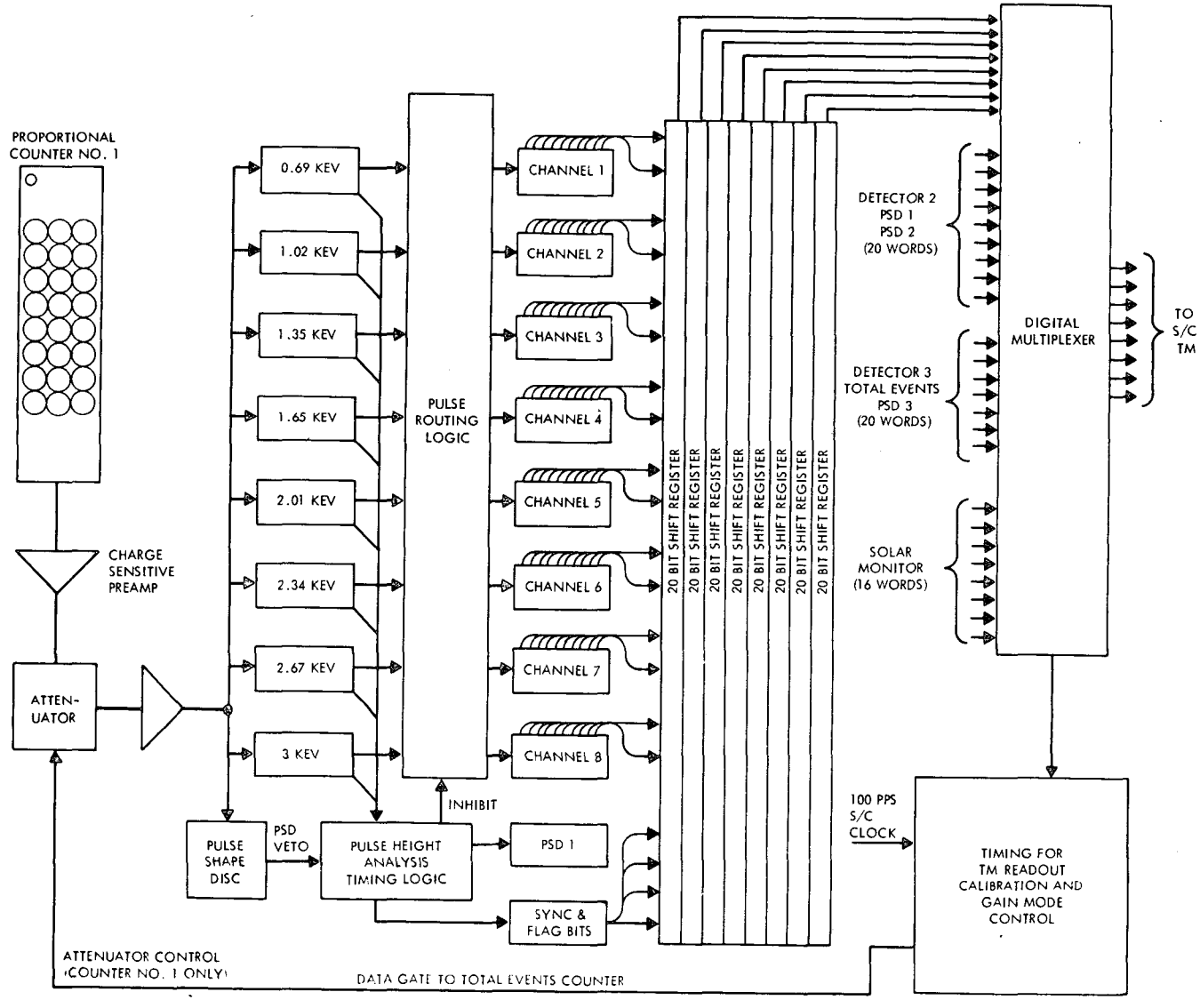

Figure 6. X-ray Spectrometer Block Diagram

The first seven channels are equal in width while the eighth channel contains the integral number of events with energies greater than channel 7. The pulses from each data channel are counted by the counters in the counter shift register logic. Every 8 seconds the contents of the counters are transferred to the shift registers, and the counters are reset. The data is then sequentially shifted out of the shift registers to telemetry at a ten word per second rate. Each TM word consists of 8 bits. Each counter is 16 bits long thereby supplying two TM words. The TM word output sequence is divided into four groups of 20 words each. They are obtained from the 20 word long shift registers which are sequentially gated through the output multiplexer by the main timing. Each pulse from the charge sensitive preamplifier is also processed by a pulse shape discriminator (PSD) which distinguishes x-ray events from background. The PSD gates off the pulse routing logic thus preventing non-x-ray events from being counted.

5. Data Format: Data transmitted from the CSM is recorded at ground stations on magnetic tape. Raw spectral data, ground navigational data and ephemeris data is thus obtained. The data obtained are relatively simple. The x-rays observed by each of the three lunar detectors are sorted out into 7 equal interval energy channels. The bare detector is operated in two modes; high gain (normal) mode and attenuate. At the initial turn on the bare detector operates for 9.87 seconds in the attenuate mode covering an approximate range of 1.5 - 5.5 Kev. At the end of this cycle the bare detector automatically goes into normal mode covering the range 0.75 - 2.75 Kev. During flight the bare detector automatically operates for 8 hours in the normal mode and two hours in the attenuate mode. The filtered surface detectors continuously cover the spectral range of 0.75 - 2.75 Kev. The solar monitor also covers an approximate range of 1 - 3 Kev.

   Ultimately then the printout tells us for each detector how many pulses of a given energy were observed in a given energy channel for a given measurement interval. From this printout one can plot histograms which are subsequently reduced by alternate techniques to line intensities and finally to chemical concentrations.

Operation of the Experiment

The x-ray experiment was turned on 84 hours into the flight, during the third revolution around the moon. From 84 to 102 hours G.E.T.* the orbit was

*G.E.T. is ground elapsed time.

approximately 8 x 60 nautical miles. During this period some 2 hours of undegraded x-ray data were obtained which will be reported on at a later date. After 102 hours the orbit was circularized and maintained at approximately 60 nautical miles until trans-earth coast. During the orbital period over 100 hours of surface measurements were made. The solar monitor detector was used for simultaneously monitoring the solar x-ray flux. Lunar backside data was recorded on magnetic tape and telemetered on the forward side. Becuase both record and playback occur in the same tape direction, it was necessary to rewind the tape recorder each time. This led to some data loss of backside information. An attempt was made to alternate the rewind operation so that it occurred either after signal loss or before signal acquisition in order to maximize the amount of ground coverage. In the x-ray experiment the data loss occurred only when the tape recorder was rewound on the illuminated portion of the hidden side. It has now become obvious that the data loss has not seriously compromised the experiment.

The data from the experiment were displayed in near real time as a numeric display on a cathode ray tube monitor. The data displayed were in the form of running sums for the seven energy channels for each of the four detectors. The data were updated at one minute intervals and at regular intervals of about four hours were supplied as hard copy printout. This preliminary report is based on the reduction of this quick look data. As a consequence of this, our results as presented, are of necessity degraded in terms of spatial resolution along the projected ground track since each minute represents a three degree longitudinal displacement. Ultimately the processing of prime data, obtained for 8 second intervals, should yield improved spatial information.

Treatment of the Data and Results

We have alternate procedures for processing the flight information depending on the degree of sophistication warranted by the data. For the following preliminary report the data has been treated in a very simple fashion based on the energy discrimination afforded by the selected x-ray filters. The following assumptions have been made:

1. All three proportional counters have identical characteristics.
2. The detectors are 100 percent efficient for the radiation transmitted through the detector window.
3. Background corrections can be made using the measured darkside fluxes.
4. The effect of x-ray scaterring on the Al/Si intensity ratios while real can be ignored in these first estimates.

Based on the above assumptions three simultaneous expressions of the folowing form were written:

$$I_{Bare} = T^{Be}_{Al} I_{Al} + T^{Be}_{Mg} I_{Mg} + T^{Be}_{Si} I_{Si} \quad (1)$$

$$I_{Al\ filter} = T^{Be}_{Al}\left(I_{Al} T^{Al}_{Al}\right) + T^{Be}_{Mg}\left(I_{Mg} T^{Al}_{Mg}\right) + T^{Be}_{Si}\left(I_{Si} T^{Al}_{Si}\right) \quad (2)$$

$$I_{Mg\ filter} = T^{Be}_{Al}\left(I_{Al} T^{Mg}_{Al}\right) + T^{Be}_{Mg}\left(I_{Mg} T^{Mg}_{Mg}\right) + T^{Be}_{Si}\left(I_{Si} T^{Mg}_{Si}\right) \quad (3)$$

$I_{Bare}, I_{Al\ filter}, I_{Mg\ filter}$ are respectively the total intensities summed over all seven channels for the bare detector, the detector with the aluminum filter and the detector with the magnesium filter.

$T^{Be}_{Al}, T^{Be}_{Mg}, T^{Be}_{Si}$ are respectively the transmission factors of the detector Be windows to the characteristic Al, Mg and Si radiation.

T^{Al}_{Al}, T^{Al}_{Mg}, etc. are respectively the transmission factors of the Al filter for the characteristic Al, Mg etc., radiation.

T^{Mg}_{Al}, T^{Mg}_{Mg}, etc. are respectively the transmission factors of the Mg filter for the characteristic Al, Mg etc., radiation.

A least square analysis method was used to solve the equations listed above. This method was chosen because estimation of statistical validity of the results are easily obtained. Solving the above equations a number of Al/Si and Mg/Si intensity ratios were obtained. It must be emphasized that these are x-ray intensity ratios and not elemental ratios. These are proportional to each other but not equal.

Observations and Results

We had pointed out in the experiment description that the flux intensity and energy distribution of the solar x-rays was expected to have a significant effect on the nature of the fluorescent x-rays. The purpose of the solar monitor was to observe the intensity and energy distribution of the solar x-rays as a function of time and simultaneously with the surface measurements. Figure 7 is a plot of the integrated intensities registered by the solar monitor for the period corresponding to the surface measurements. These were the values observed at the subsolar point. For comparison a plot is also shown for the surface intensities as observed with the bare detector. Except for two exceptions, orbits

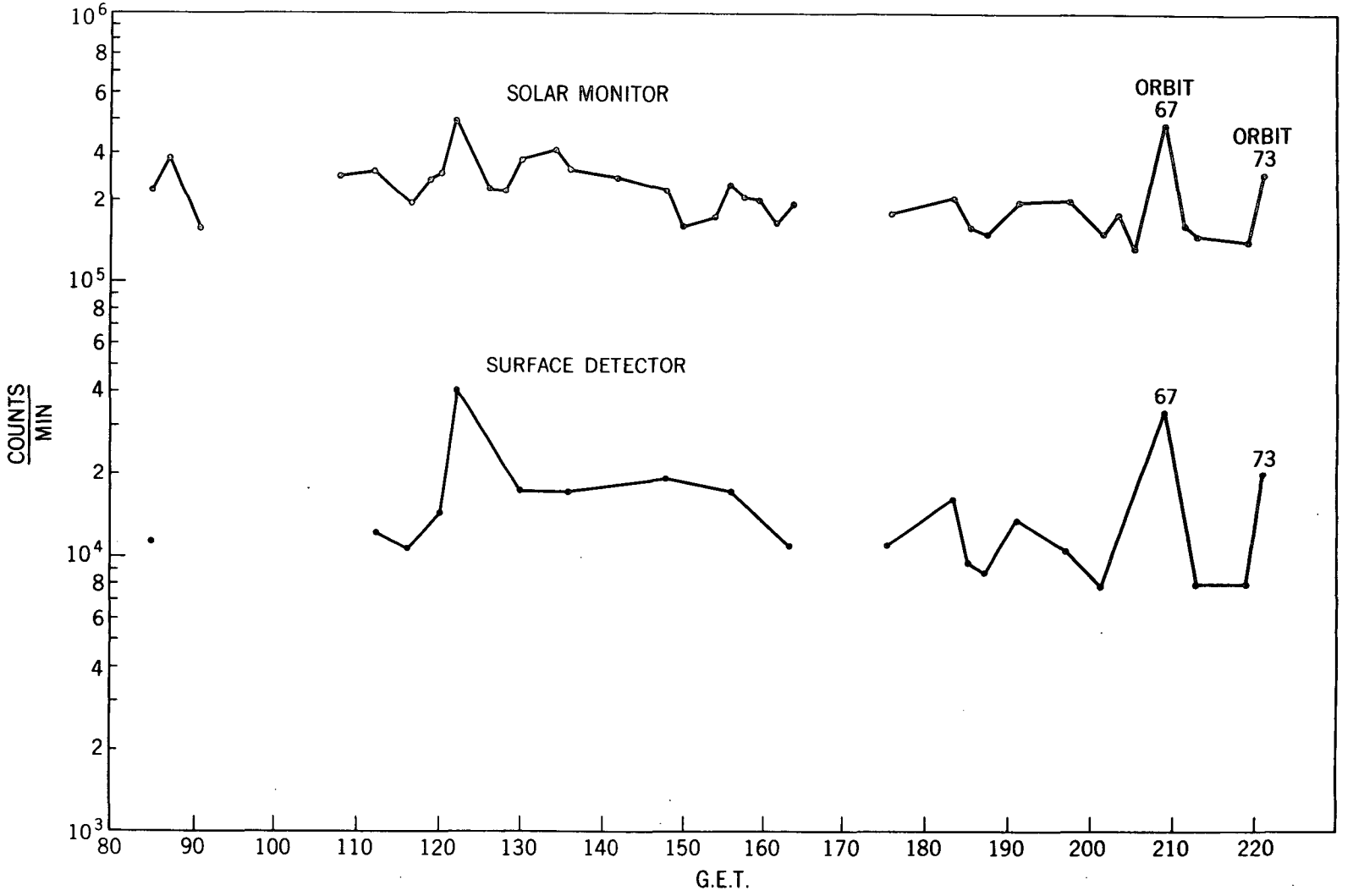

Figure 7. Comparison of Solar X-ray Flux and Surface Flux

67 and 73, the solar flux was fairly stable, not varying by more than ±30% of the mean value. This stability was equally reflected in the surface data which not only indicates a stable incident flux but also a stable spectral distribution.

During orbits 67 and 73 there was a marked increase in flux and apparently a hardening of the energy spectrum. This was reflected in reduced Al/Si ratios due probably to enhanced excitation of the Si. On subsequent revolutions the solar flux intensity returned to more normal values as did the Al/Si ratios.

In Figure 8 we have plotted Al/Si intensity ratios along the ground tracks corresponding to revolutions 16, 25-27, 37, 63-64 and 72. Because of the close overlap it was found useful to average some of the orbits such as 25, 26, and 27 and 63-64. The agreement between values on the close ground tracks was about ±10 percent on the average.* Examining the ground tracks in a direction from east to west the spacecraft is seen to have overflown such features as the craters Gagarin and Tsiokolvsky, the backside and eastern limb highlands, the mare areas Smythii, Crisium, Fecunditatis, Tranquillitatis and Serenitatis, the Haemus Mts., the Apennines, Mare Imbrium and Oceanus Procellarum. It is obvious that there are very marked differences between the eastern limb highlands and the mare areas, the Al/Si intensity ratios varying by more than a factor of two, being lowest in the mare areas.

These values are detailed in Table 1 and plotted synoptically in Figures 9 and 10. Figure 9 represents a northerly trajectory (revs. 16, 26-28, 34) and Figure 10 a more southerly course (revs. 63-64, 72). The observations that one can make are as follows:

1. The Al/Si intensity ratios are lowest over the mare areas and highest over the terrae (average of 0.67 vs 1.13). The extremes vary from 0.58 to 1.37, a factor of over 2.3.

2. The Apennine region gives a value of 0.88 and the Haemus Mts. a lower average value of 0.83. On the other side of the Apennines (the Archimedes Rille area) the observed value is 0.64. On either side the values for Imbrium and Serenitatis are 0.59 and 0.58. The Apennines have values in between the mare and the eastern limb highlands.

3. Examining the Al/Si coordinate plot we see a general tendency for the values to increase from the western mare areas to the eastern limb highlands.

*The scatter is based on a one sigma variation calculated by taking repetitive values for a given area.

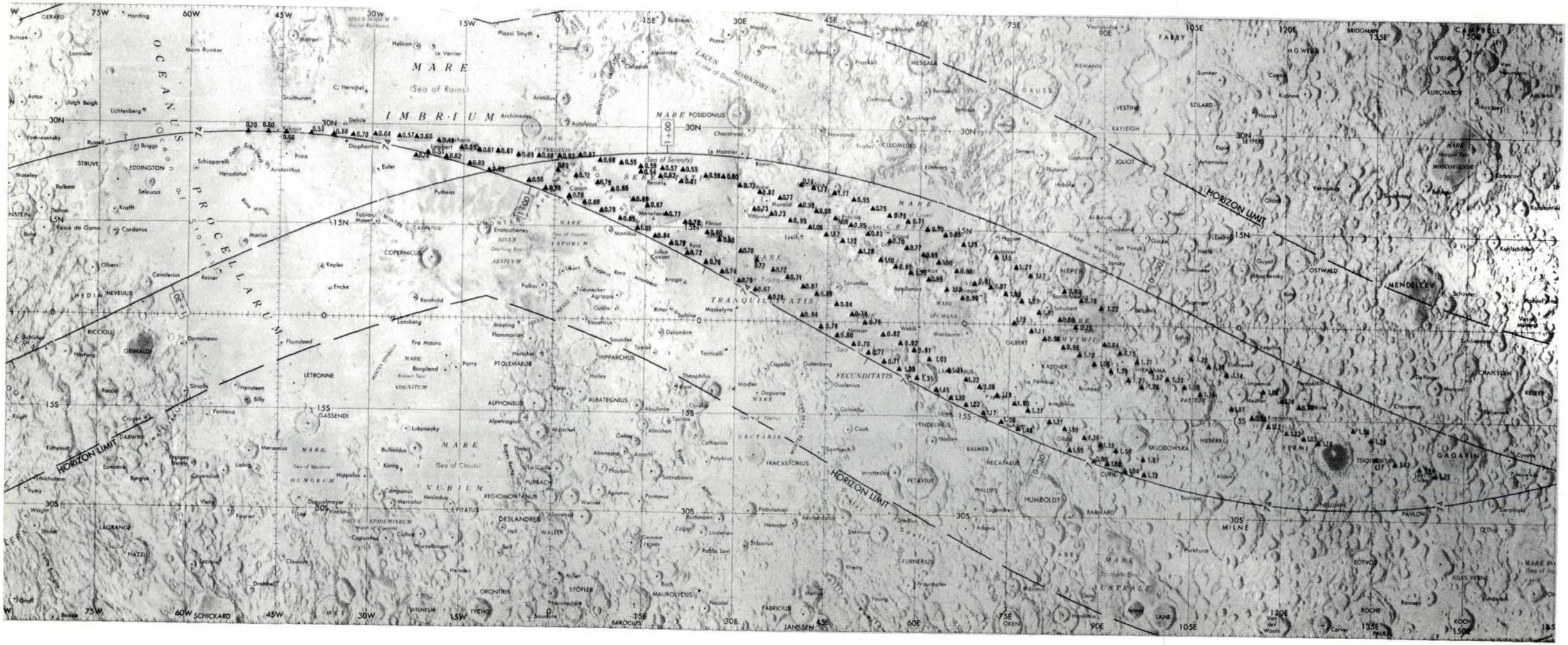

Figure 8. Al/Si intensity ratios along selected ground tracks

Table 1

Si/Al Intensity Ratios For Various Lunar Features

Features	
Mare Serenitatis	0.58 ±0.06 RIM 0.71 ±0.05
Imbrium	0.59 ±0.04
Crisium	0.71 ±0.02 RIM 0.80 ±0.09
Tranquillitatis	0.71 ±0.05 RIM 0.84 ±0.04
Fecunditatis	0.73 ±0.07 RIM 0.94 ±0.14
Smythii	0.73 ±0.07 RIM 1.00 ±0.11
Archmides Rille Area	0.64 ±0.03
Apennine Mts.	0.88 ±0.03
Haemus Mts.	0.83 ±0.10
Highlands E. of Serenity to 40 E	0.80 ±0.08
Highlands W. and S.W. of Crisium	1.08 ±0.13
Highlands between Crisium and Smythii	1.07 ±0.11
Highlands between Smythii and Tsiolkovsky	1.16 ±0.11
Highlands E. of Fecunditatis	1.29 ±0.23
Highlands E. of Tsiolkovsky	1.37 ±0.25
Area N. of Schroter's Valley	0.73 ±0.05
Area N.E. of Schroter's Valley	0.64 ±0.09

4. The rim areas as one would predict are intermediate between the mare areas and the surrounding highlands.

In Figures 11 and 12 we see another interesting correlation between Al/Si ratios and albedo values along selected ground tracks. Generally the higher Al/Si ratios correspond to higher albedo values. There are occasional deviations from these relationships due to surface features (as for example the Copernican type crater identified in the plot in Figures 11 and 12. It thus appears that one

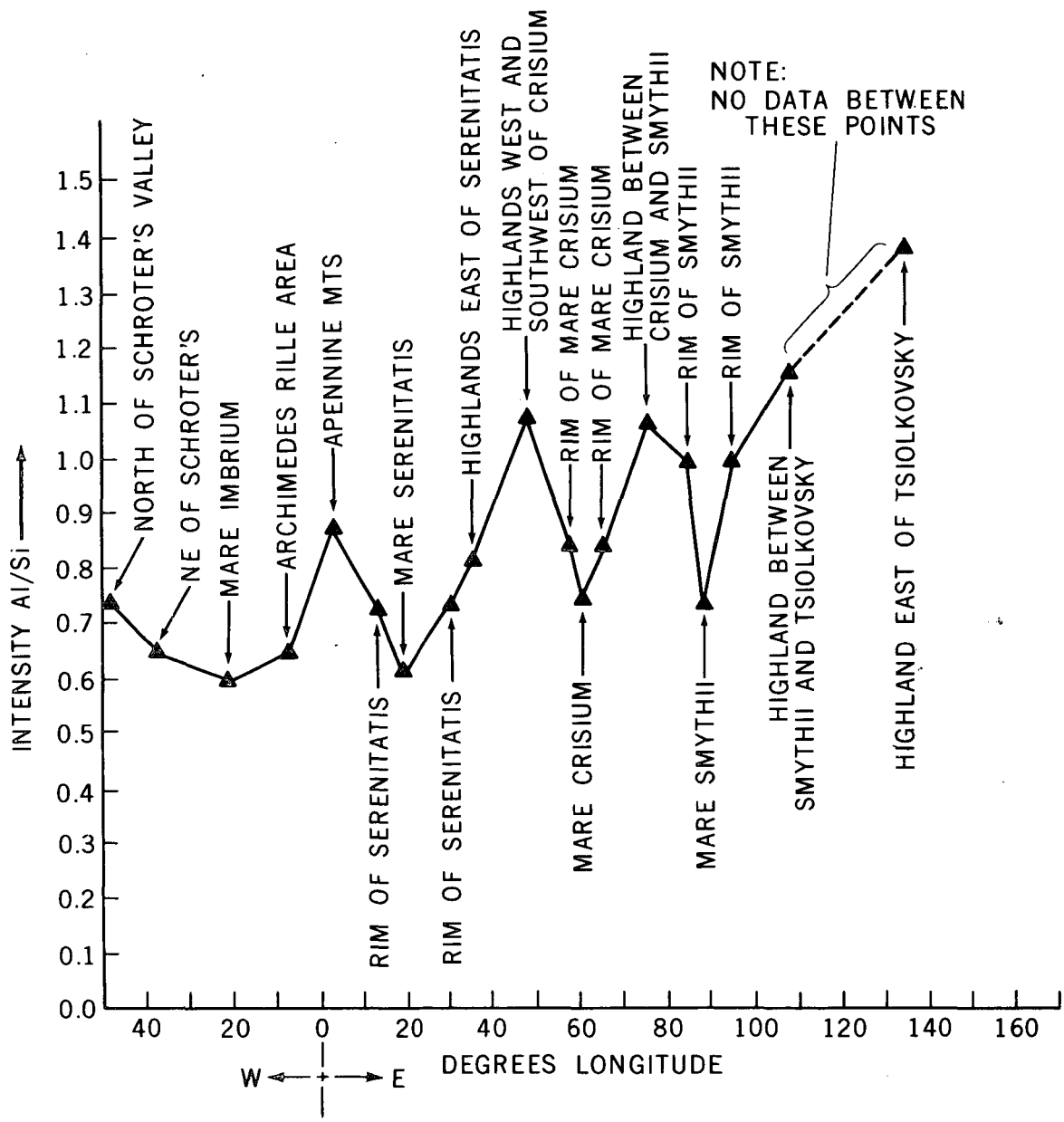

Figure 9. Plot of Al/Si Ratios Along a Northerly Ground Track

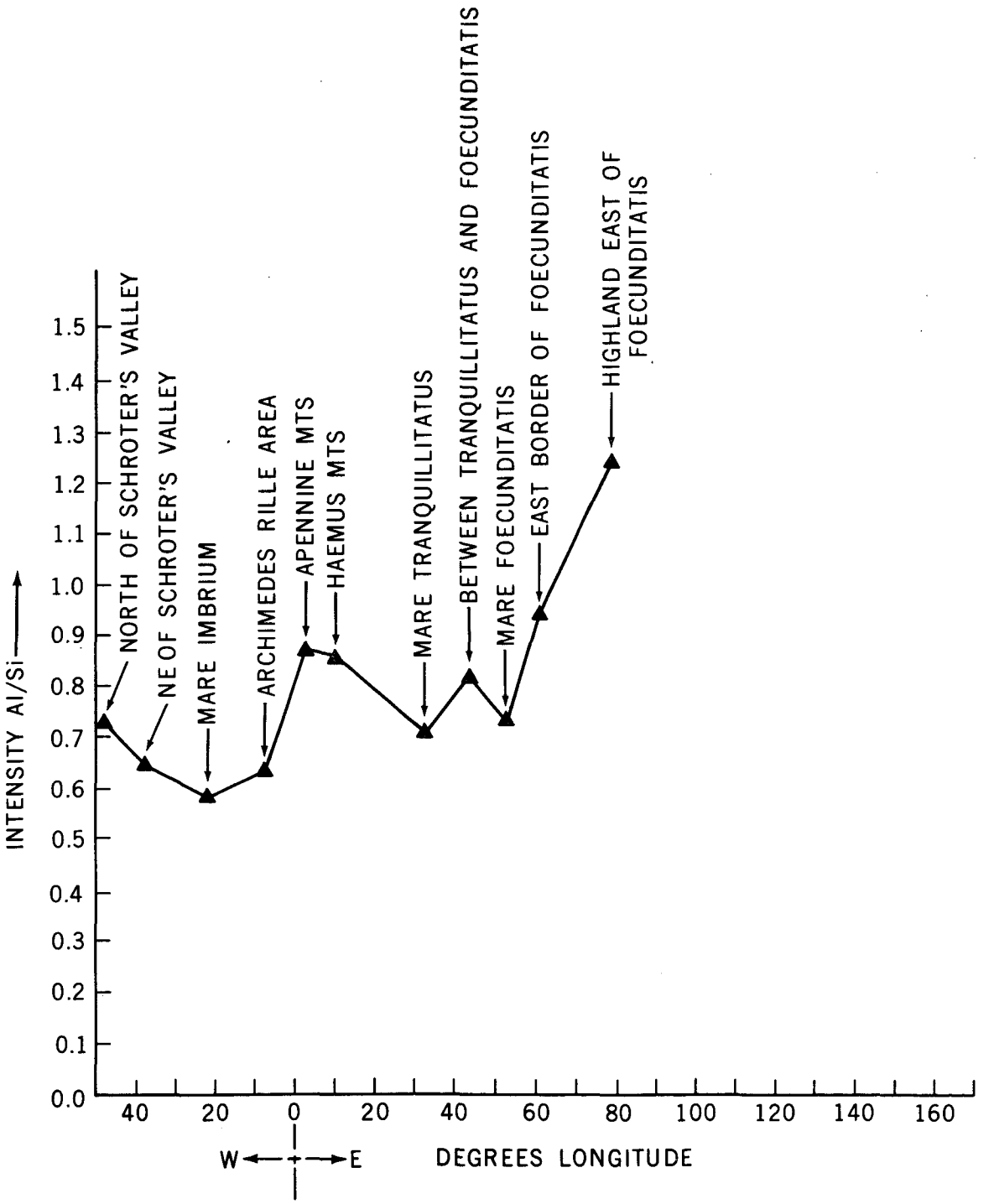

Figure 10. Plot of Al/Si Intensity Ratios Along a Southerly Ground Track

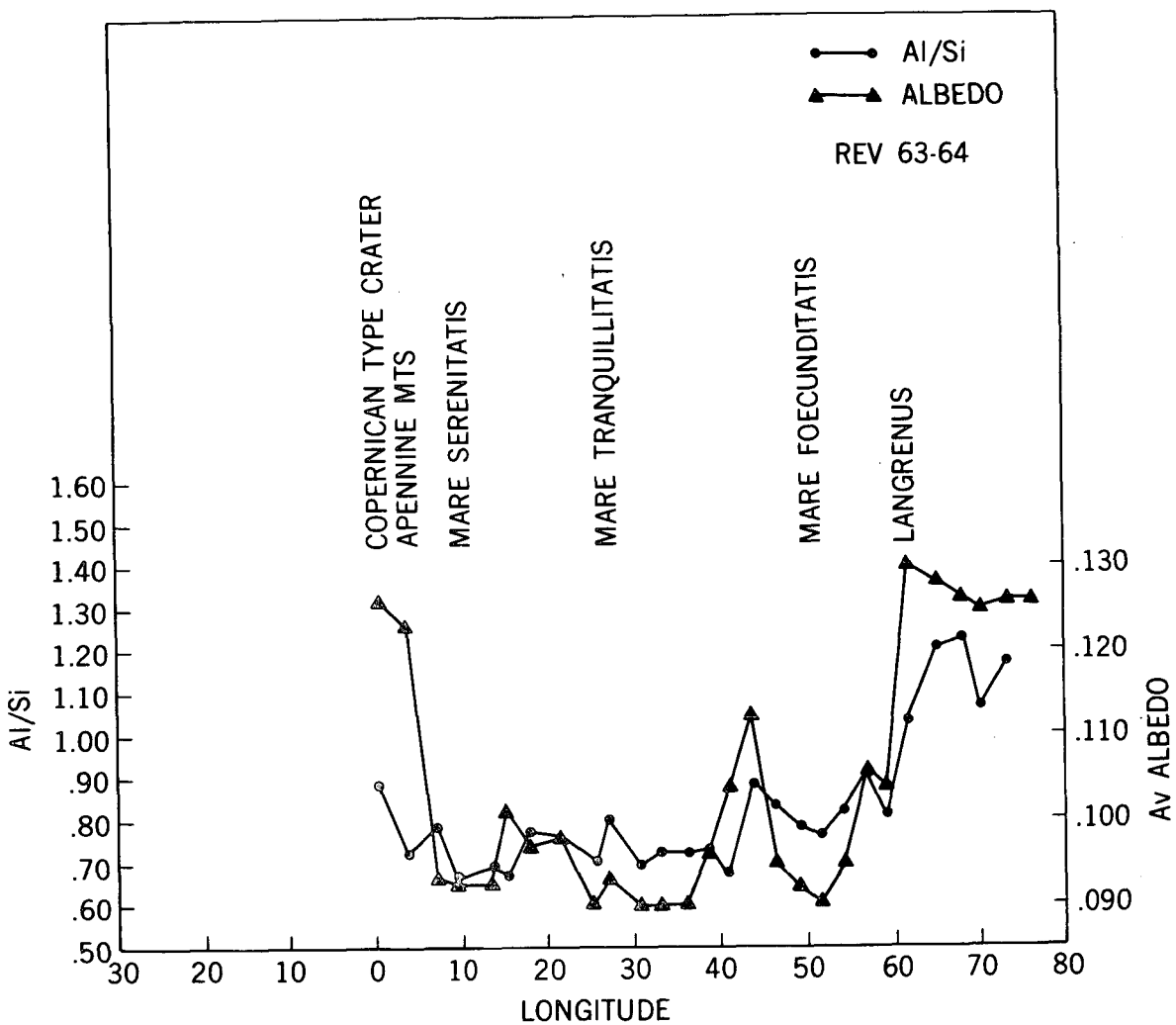

Figure 11. Plot of Al/Si intensity ratios vs normal albedo values (2). Albedo values are for points corresponding to average Al/Si intensities for readout intervals shown on map, for revolutions 63 and 64. (See Figure 13.)

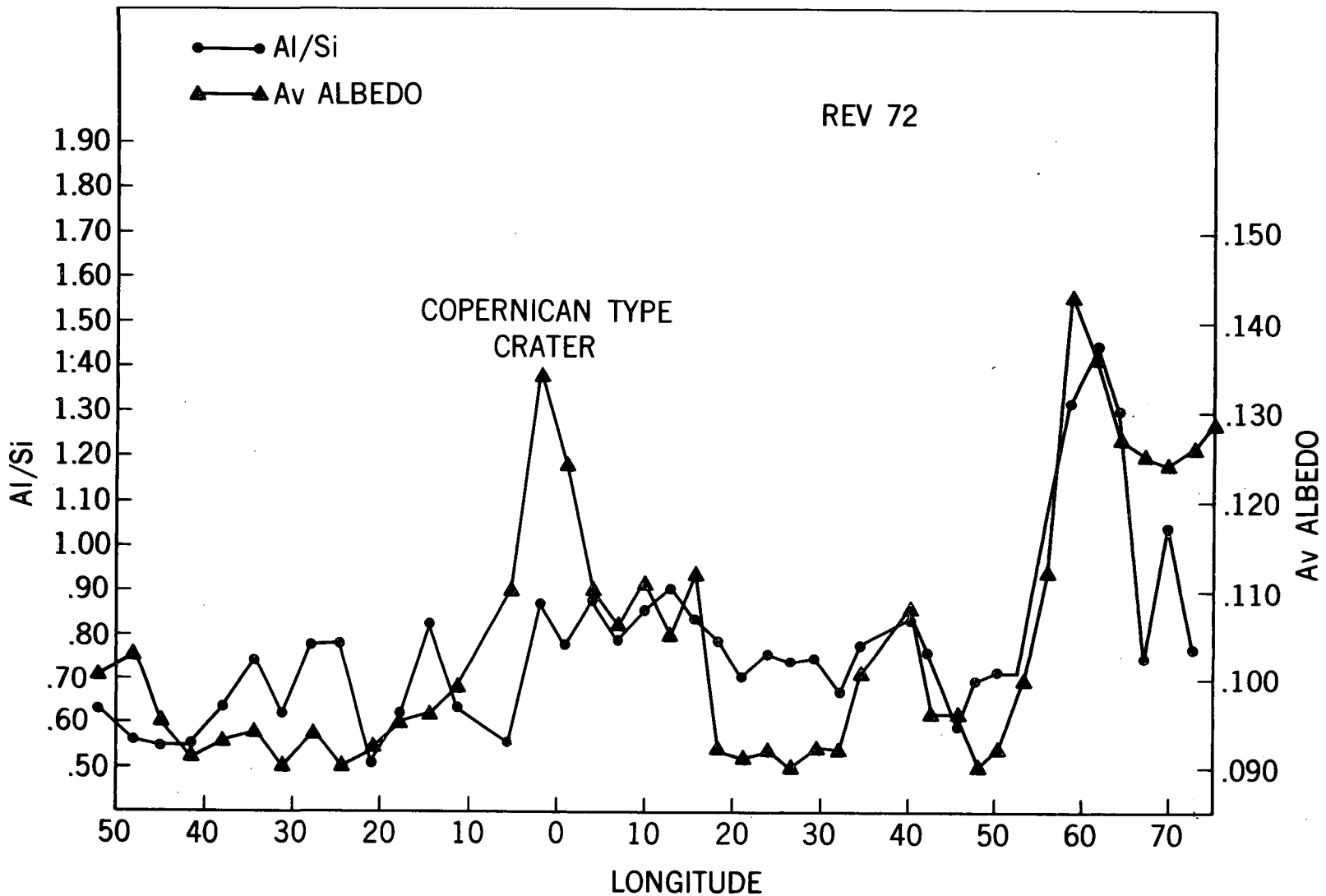

Figure 12. Comparison of Albedos and Al/Si Ratios for Revolution 72

Figure 13. Full moon telescopic photograph emphasizing albedo differences of earthward side. For landmarks, see map; maria labeled as follows: M. Serenitatis (S), M. Crisium (C), M. Tranquillitatis (T). Photograph from Lick Observatory, by Moore and Chappel, 36 inch refractor, Jan. 17, 1946.

can use the x-ray data to infer something about the composition of areas with different albedos. It is possible, for example to state whether the albedo variations are related to chemical differences or rather to the nature and perhaps age of a given feature.

There are other interesting correlations but the comments on these are of necessity of a very preliminary nature. An attempt has been made to plot Al/Si intensity ratios along a gravity profile determined by Sjogren and described elsewhere in this report (3). The observed correlation is that the Al/Si ratios varies inversly with the gravity values. For example, the lowest Al/Si ratios are found in the regions of greatest positive anomalies.

Finally an attempt has been made to arrive at actual concentration ratios for Al/Si. The approach to determining these concentrations is in part theoretical and in part empirical. The theoretical calculations are based on the assumption of a quiet sun and a coronal temperature of 4×10^6 deg. K. These conditions give an x-ray energy distribution consisting of both a continuum and characteristic lines which is consistent with our solar monitor observations shown normalized in Figure 14. Using this distribution and various compositions of soils as determined from the analysis of lunar samples we have been able to calculate a relationship between Al/Si intensity ratios as a function of chemical ratios.

Empirically, we have assumed soil values from the Apollo 11 site at Tranquillity Base and Luna 16 values from Fecunditatis to be ground truth values. With these values and the theoretically calculated slopes we have been able to determine the values of Al/Si concentrations shown in Table 2 for various parts of the moon along the ground track. Included in this table are some typical values for various lunar rocks determined by the chemical analysis of lunar materials.

Discussion of Results

The results of the S 161 experiment are still in the preliminary stages of analysis. Nevertheless, some tentative interpretations are possible, especially when the data are viewed in the context of previous Apollo missions. These interpretations are based on comparison of the relative aluminum/silicon ratios with albedo, regional geology, and analyses of returned samples. They are subject, at this stage of analysis, to several limitations. First, the data plotted were read out at one-minute intervals; this, and the 60° field of view of the x-ray spectrometer, mean that the Al/Si ratios refer to large areas. Second, the S-161 experiment is inherently a surface compositional measurement, providing no information, except for the mixing effect of "gardening", on the subsurface composition below depths of about 0.1 millimeter.

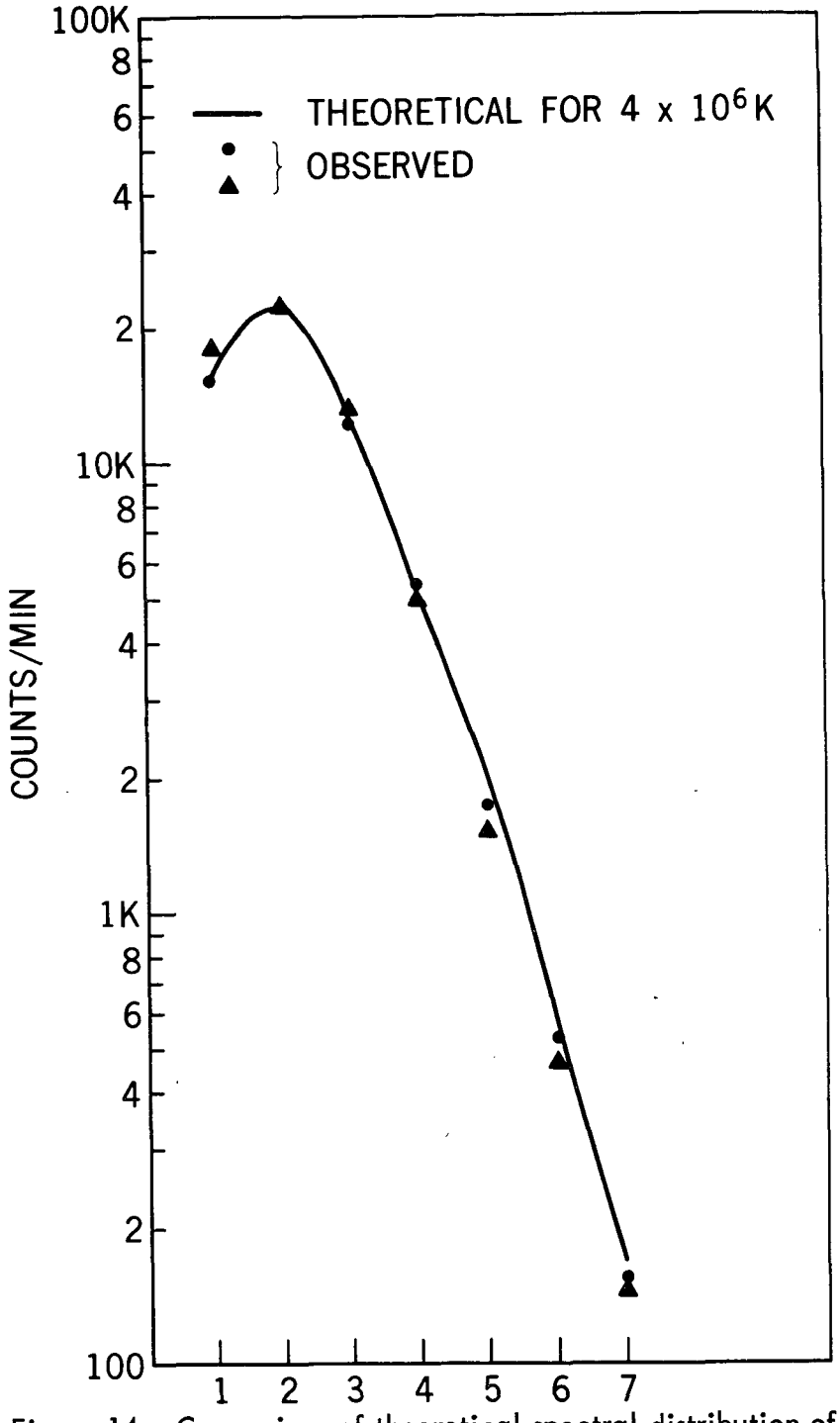

Figure 14. Comparison of theoretical spectral distribution of detector with radiation 36° from normal with solar monitor data taken ±12 minutes from subsolar point.

Table 2

Al/Si Concentrations Ratios Calculated from the Intensity Ratios of Table 1

Mare Serenitatis	0.29 ±0.02
Mare Imbrium	0.29 ±0.04
Mare Crisium	0.37 ±0.01
Mare Tranquillitatis	0.36 ±0.03
Mare Fecunditatis	0.38 ±0.04
Mare Smythii	0.37 ±0.05
Archimedes Rilles Area (to Marsh of Decay)	0.32 ±0.02
Apennines Mts.	0.48 ±0.01
Haemus Mts.	0.44 ±0.06
Highlands E. of Serenitatis to 40 E	0.42 ±0.05
Highlands W. and S. of Crisium	0.60 ±0.07
Highlands between Crisium and Smythii	0.59 ±0.07
Highlands between Smythii and Tsiolkovsky	0.65 ±0.09
Highlands E. of Fecunditatis	0.73 ±0.14
Highlands E. of Tsiolkovsky	0.78 ±0.15
Area N. of Schroter's Valley	0.37 ±0.04
Area N.E. of Schroter's Valley	0.32 ±0.06
Apollo 11, Mare Tranquillitatis Bulk Soil (7)	0.37
Surveyor, Mare Tranquillitatis Regolith (8)	0.35
Apollo 12, Oceanus Procellarum Average of Soils (9)	0.325
Luna 16, Mare Fecunditatis Bulk Soil (10)	0.416
Surveyor VI, Sinus Medii, Regolith (8)	0.338
Surveyor VII, Rim of Tycho, Regolith (8)	0.546
Apollo 14, Fra Mauro, Soils (11)	0.413
Apollo 15, Hadley Rille-Apennines, Soils (3 preliminary) (12)	0.379
Apollo 11 and 12 Anorthositic Gabbros	0.637

Table 2 (continued)

Gabboric Anorthosites	0.819
Anorthosite	0.885
Apollo 12, Noritic Materal (13)	0.416
Apollo 12, Kreep (14, 15)	0.394
Apollo 12, Dark 12013 (14, 15)	0.327

Subject to these limitations, we draw the following general conclusions about the moon's geology and evolution from the x-ray experiment.

1. The Al/Si ratios (Tables 1 and 2) confirm that the highlands and maria do indeed have different chemical and mineralogical compositions. This conclusion, though expected, should be stated explicitly since there have been to date only two sample return missions (Apollo 14 and 15) to the highlands. Furthermore, it confirms that the albedo difference between highlands and maria Figures 11 and 12 is at least partly the expression of chemical difference. The x-ray experiment, with the evidence from returned samples, suggests that there are two major types of materials exposed. The high aluminum content of the highlands suggests they are related to the anorthositic or noritic fractions of returned samples, while the low aluminum content of the maria is consistent with the composition of the many mare basalts analyzed (Table 2).

   The distinct compositional differences found between the maria and the highlands puts limits on the effectiveness of horizontal transport of material, in particular by electrostatic suspension of fine particles. Were such a mechanism effective for long distance transport, the x-ray experiment would probably not detect compositional differences between highlands and maria, since it "sees" only the fine-grained surface material that would be widely distributed by electrostatic suspension There has been perhaps some blurring of the mare-highland contacts, as will be discussed in conclusion 3, probably by the cumulative effect of minor impacts. But it seems clear that horizontal transport, by this mechanism or by electrostatic suspension, has not carried material farther than about a tenth the diameter of, for example, Mare Serenitatis. This finding incidentally reinforces the argument frequently put forth against electrostatic transport, namely the persistence of albedo differences, since the x-ray intensities so far correlate well with albedo.

2. As shown in Table 2, there is some indication of chemical differences among maria; the raw data suggest that the circular maria are relatively lower in aluminum than the irregular maria. If real, these differences may throw light on the origin of the mare basins, since the circular maria are characterized by mascons and apparent ejecta blankets, while the irregular maria are not. The S-161 data require more refinement to confirm this conclusion. However, it is in agreement with the recent work of Soderblom (4), who found that the circular maria ("red") could be distinguished spectrally from the irregular maria ("blue").

3. There appear to be systematic chemical variations within individual maria, in particular M. Crisium and Serenitatis. The raw data suggest that the edges of these maria are relatively higher in aluminum than the centers. These variations may be real, a possibility supported by the systematic albedo patterns in Mare Serenitatis Carr (5) and more indirectly by the work of Soderblom (4), who found several spectral subtypes of both "red" and "blue" maria. However, two factors confuse the picutre at this time. First is the field of view; intensity readings near mare rims may include highland areas. Second, the mare regolith near the orders may contain substantial amounts of ejecta from the nearby highlands. Study of x-ray data taken at 8 second intervals may clarify this result.

4. The Imbrium ejecta blanket (Fra Mauro and Alpes Formations (Wilhelms and McCauley, (6)) and possibly other may be chemically different from the highlands outside such ejecta blankets. The intensity ratios suggest that they are intermediate in aluminum content between the maria and the non-ejecta highlands. An obvious interpretation of this difference, assuming it to be real, is that the mare basin ejecta blankets represent more basic material derived from some depth in the moon. However, the ejecta blanket areas covered by the x-ray spectrometer, in particular in the Haemus Mountains south of Mare Serenitatis, included substantial areas of highland mare material (shown as Eratosthenian mare by Wilhelms and McCauley). It is thus unwise at this time to draw firm conclusions about the composition of the mare ejecta.

5. The x-ray experiment supports the belief that the moon has a global, differentiated, aluminum-rich crust, whose formation was the first major geochemical event of the moon's geologic evolution after its formation. Despite the preliminary nature of these data, one can pinpoint areas on the lunar highlands which have aluminum/silicon ratios corresponding to analyzed lunar materials of anorthositic affinity (to use the term suggested by Wood, et al.). As shown in Table 2, the anorthositic gabbros have an Al/Si ratio of 0.64, gabbroic anorthosites 0.82, and anorthositic fragments 0.89. From the S-161 concentration ratios

shown in Table 2, it can be seen that the "anorthositic" material could be derived from any of several distinct highland areas on or near the moon's east limb. This is not, of course, to exclude other highland surfaces for the actual source of these materials, but to emphasize that there are large definite areas from which they could be derived.

Added to this positive evidence for a crust of anorthositic affinity is the negative evidence, from the Apollo 15 gamma ray experiment and from Luna 10, that the highlands do not have large amounts of granitic material, which would otherwise be a possible explanation for the higher aluminum content of the highlands. Other negative evidence is the scarcity of granitic compositions in samples returned to date by Apollos 11, 12, and 14, and Luna 16.

Summary

Preliminary analysis of only part of the S-161 experiment data, pertaining to the relative aluminum/silicon ratios, shows that the experiment has been highly successful. Major compositional differences between the maria and highlands have been confirmed, and there are suggestions of compositional variations within both maria and highlands. The compositions inferred from the x-ray and gamma-ray data are consistent with the study of returned lunar samples. The main preliminary results of the S-161 experiment is tentative confirmation that the moon has a differentiated highland crust of feldspathic composition, probably similar to the various materials of anorthositic affinity found in samples from Apollo 11, 12, 14 and 15.

References

1. Adler, I., X-ray Emission Spectrography in Geology, 1966, Elsevier.

2. Pohn, H. A., and Wildey, R. L., A photo-electric-photographic study of the normal albedo of the moon, Geological Survey Professional Paper, 559-E, U.S. Geological Survey, Washington, D.C.

3. Sjogren, W. L., Private Communication.

4. Soderblom, L. A., The distribution and relative ages of regional lithologies, in the lunar maria (abstract), P. 690-691, Abstracts with Programs, V. 2, No. 70, Geological Society of America, 1970 Annual Meeting.

5. Carr, M. H., Geologic Map of the Mare Serenitatis region of the moon, U.S. Geological Survey, Misc. Geol. Inv. Map I-489.

6. Wilhelms, D. E., Summary of telescopic lunar stratigraphy in lunar and planetary investigation, Part A of Astrogeologic studies annual progress report, July 1, 1965 to July 1, 1966. U.S. Geological Survey Open File Report p. 235-298.

7. Proc. Apollo 11 Lunar Sci. Conf., Geochim. Cosmochima. Acta Supp. 1, Vol. 1-3, A. A. Levinson, ed., Pergamon Press, 1970.

8. Mason, B., and Melson, W. G., The Lunar Rocks. Wiley, 1970, p. 11.

9. Proc. of the Second Lunar Sci. Conf., Houston, January 1971.

10. Vinogradov, A. P., Preliminary Data on Lunar Ground Brought to Earth by Automatic Probe "Luna - 16". Proc. of the Second Lunar Sci. Conf., Houston, January 1971.

11. Preliminary Examination of Lunar Samples from Apollo 14., Science, Vol. 173, No. 3998, Aug. 20, 1971, pp. 681-693.

12. Private Communications.

13. Wood, J. A.; Marvin, U.; Reid, J. B.; Taylor, G. J.; Bower, J. F.; Powell, B. N.; and Dickey, J. S., Jr. Relative Proportions of Rock Types, and Nature of the Light-Colored Lithic Fragments in Apollo 12 Soil Samples. Proc. of the Second Lunar Sci. Conf., Houston, January 1971.

14. McKay, D.; Morrison, D.; Lindsay, J.; and Ladle, G. Apollo 12 Soil and Breccia. Proc. of the Second Lunar Sci. Conf., Houston, January 1971.

15. Meyer, C., Jr.; Aitkin, F. K.; Brett, R.; McKay, D. S.; and Morrison, D. A. Rock Fragments and Glasses Rich in K, REE, P in Apollo 12 Soils: Their Mineralogy and Origin. Proc. of the Second Lunar Sci. Conf., Houston, January 1971.